Check for updates

The role of ordering on the thermoelectric properties of blends of regioregular and regiorandom poly(3-hexylthiophene)

Eunhee Lim[†], Anne M. Glaudell[†], Rachel Miller[§], Michael L. Chabinyc[†]*

† Materials Department, University of California, Santa Barbara, California 93106, United States

§ Department of Materials Science and Engineering, Cornell University, Ithaca, New York, 14850, United States

Corresponding Author

* E-mail: mchabinyc@engineering.ucsb.edu

Author Manuscript

This is the author manuscript accepted for publication and has undergone full peer review but has not been through the copyediting, typesetting, pagination and proofreading process, which may lead to differences between this version and the Version of Record. Please cite this article as doi: 10.1002/aelm.201800915.

This article is protected by copyright. All rights reserved.

Author Manuscript

ABSTRACT

The thermoelectric properties of semiconducting polymers are influenced by both the carrier concentration and the morphology that sets the pathways for charge transport. A combination of optical, morphological, and electrical characterization was used to assess the effect of the role of disorder on the thermoelectric properties in thin films of poly(3-hexylthiophene) (P3HT) doped with 2,3,5,6-tetrafluoro-7,7,8,8-tetracyanoquinodimethane (F_4TCNQ). Controlled morphologies were formed by casting blends of regioregular (RR-P3HT) and regiorandom (RRa-P3HT) and then subsequently doping with F_4TCNQ from the vapor phase. Optical spectroscopy and *X*-ray scattering show that vapor phase doping induces order in the disordered regions of thin films and increases the long-range connectivity of the film. The thermoelectric properties were assessed and show that while the Seebeck coefficient is affected by structural ordering, the electrical conductivity and power factor are more dominantly correlated with the long-range connectivity of domains.

Introduction

The thermoelectric properties of semiconducting polymers are a strong function of their carrier concentration. The addition of charge carriers increases the electrical conductivity (σ) of the polymer by the fundamental relationship $\sigma = qn\mu$, where q the charge of an electron, n is carrier concentration, and μ is carrier mobility. Electrical doping of semiconducting polymers is frequently accomplished by charge transfer between a molecular dopant and the polymer.[1–4] The offset between ionization energy and electron affinity of the two materials works as a driving force for charge transfer to form carriers. Due to structural and electronic disorder, both the efficiency of charge transfer with dopants

This article is protected by copyright. All rights reserved.

2199160x, 2019, 11, Downloaded from https://onlinelibrary.wiley.com/doi/10.1002/aelm.201800915, Wiley Online Library on [22/02/2024]. See the Terms and Conditions (https://onlinelibrary.wiley.com/terms-and-conditions) on Wiley Online Library for rules of use; OA articles are governed by the applicable Creative Commons License

and the carrier mobility in polymers is a function of the concentration of the dopant. These factors make it difficult to predict the change in electrical conductivity with *n*.[5] The thermopower, i.e. Seebeck coefficient, also has a complicated relationship with carrier concentration because of changes in the shape of the electronic density of states (DOS) near the Fermi level with charge carrier concentration.[6] Unraveling how both the electrical conductivity and thermopower evolve with doping is an important challenge for the development of thermoelectric polymers.[7]

The doping method affects the thin film structure of polymers and, consequently, the thermoelectric performance because charge transport is impacted by crystalline order and also the longer range morphology.[7,8] The electrical conductivity is largely dependent on the process used for doping and the resulting morphology, while the Seebeck coefficient has a weaker dependence on processing.[10] Controlling the morphology of solution-cast doped films is difficult due to the interaction between the polymer and dopant in solution due to changes in the solvent quality upon charge transfer. Post-processing such as thermal, or solvent annealing, is also challenging because volatile dopants can be driven out of the film. An alternative processing method is sequential doping where a neat polymer film is cast and then the dopant is allowed to infiltrate the film from a solvent, or by solid-state diffusion of a vapor. Sequential processing, particularly from vapor, has been shown to help preserve the morphology of the neat film.[8,9,11] Processing methods that are known to enhance the field-effect mobility in transistors can therefore be used to set the morphology of the neat film. Compared to solution doped films, a ten to a hundred-fold increase in electrical conductivity is observed in vapor doped films of semiconducting polymers, such as poly(3-hexylthiophene) (P3HT) and co-polymers of thiophene and thienothiophene (PBTTT).[10,12–14]

The effect of post-deposition of dopants on ordered and disordered domains of semiconducting polymers is necessary to understand their resulting properties. The structure of aggregates and their connectivity in films is known to strongly modify charge transport in semiconducting polymers.[15,16] This feature makes understanding the behavior of model polymers, like P3HT, particularly

This article is protected by copyright. All rights reserved.

Author Manuscript

2199160x, 2019, 11, Downloaded from https://onlinelibrary.wiley.com/doi/10.1002/aelm.201800915, Wiley Online Library on [22/02/2024]. See the Terms and Conditions (https://onlinelibrary.wiley.com/terms-and-conditions) on Wiley Online Library for rules of use; OA articles are governed by the applicable Creative Commons License

challenging. The structural order in P3HT can be controlled through the choice of solvent and deposition conditions. Using P3HT and the molecular dopant 2,3,5,6-tetrafluoro-7,7,8,8-tetracyanoquinodimethane (F_4TCNQ) as a model system, a recent study showed that the electrical conductivity and thermoelectric power factor increase with an increase in crystalline order due to improved charge mobility.[17] The Seebeck coefficient showed a more complicated relationship with crystalline order because of the formation of new states in bandgap from planarization of backbone and an increase in mobile charge carriers upon doping.[17] In another study, thin films with varying degree of crystallinity were cast from blends of regioregular (RR-) and regiorandom (RRa-) P3HT solutions and sequentially doped from an orthogonal solvent. With a combination of infrared spectroscopy and theoretical simulations, it was shown that dopants in the amorphous regions of the film lead to an increase in conjugation length and film connectivity, improving electrical conductivity at low doping levels.[18] Despite these advances, it is still unclear how the connectivity of the domains and the changes upon introduction of the dopant lead to the resulting thermoelectric properties.

In this study, we use a combination of optical, morphological, and electrical characterizations to assess the effect of the role of disorder on doping efficiency, doped film morphology, and thermoelectric properties in thin films of P3HT doped with F_4TCNQ. By using blends of RR-P3HT and RRa-P3HT to control the structural order in neat films and subsequently doping with F_4TCNQ from the vapor phase, we form electrically conductive films with controlled morphologies. Optical spectroscopy and X-ray scattering show that vapor phase doping induces order in the disordered regions of thin films and increases the long-range connectivity of the film. The thermoelectric properties were assessed and show that while the Seebeck coefficient is not a strong function of morphology, the conductivity and power factor are strongly correlated with the long-range connectivity of domains.

This article is protected by copyright. All rights reserved.

Author Manuscript

2199160x, 2019, 11, Downloaded from https://onlinelibrary.wiley.com/doi/10.1002/aelm.201800915, Wiley Online Library on [22/02/2024]. See the Terms and Conditions (https://onlinelibrary.wiley.com/terms-and-conditions) on Wiley Online Library for rules of use; OA articles are governed by the applicable Creative Commons License

Results and discussion

UV-Vis spectra show control over the fraction of ordered aggregate in neat films. To determine the structural order in blended films of RR- and RRa-P3HT as a function of composition, we used optical spectroscopy based on the known assignments of the spectral features. The absorbance spectrum of RR- P3HT has peaks at 2.0 and 2.2eV assigned to (0-0) and (0-1) vibronic transitions of ordered aggregates of the polymer **(Figure 1(a)** and **Figure S1**).[19] RRa-P3HT has a blue-shifted main absorbance at 2.7eV attributed to a lower conjugation length of the backbone than in RR-P3HT. [20] The absorbance spectra of thin films of the blends can be reproduced with a linear combination of the RR- and RRa- spectra.[21] All of the blends have vibronic peaks corresponding to 0-0 and 0-1 transition, indicating that crystallization is not completely hindered from addition of RRa- P3HT.

The fraction of aggregates in blended films of RR- and RRa-P3HT was controlled by the composition in the casting solution. We calculated the fraction of aggregates using a modified Frank-Condon fit to the optical spectrum,[22] and found it to range from 0 in 100% RRa- to 0.56 in 100% RR- films (**Figure 1(b)).** The fraction of aggregates in the RR-P3HT film is similar to the highest values from previous studies on high molecular weight RR- P3HT films calculated using X-ray scattering, NMR, and DSC.[23,24] The fraction in RR-P3HT can be controlled by changing solvents, but here we choose a common solvent for all compositions. The choice of blending RR- and RRa-P3HT gives wider range of the fraction of aggregates compared to the literature range (0.33 to 0.46) by varying solvent.[17] This control provides a means to study the role of aggregates on charge transport in doped films.

The aggregates in RR- : RRa-P3HT blend films have a narrow range of exciton bandwidths indicating that interchain order and conjugation length are relatively insensitive to blending. The interchain order and conjugation length of aggregates was analyzed by fitting the optical spectra according to the Spano model (assuming Huang-Rhys factor of 1) (Eq. 1 where A_{0-0} and A_{0-1} are

This article is protected by copyright. All rights reserved.

Author Manuscript

2199160x, 2019, 11, Downloaded from https://onlinelibrary.wiley.com/doi/10.1002/aelm.201800915, Wiley Online Library on [22/02/2024]. See the Terms and Conditions (https://onlinelibrary.wiley.com/terms-and-conditions) on Wiley Online Library for rules of use; OA articles are governed by the applicable Creative Commons License

the area of vibronic peaks from absorption spectra, W is the free exciton bandwidth of aggregates, and E_p is the intramolecular vibrational energy (= 0.18 eV)) (**Figure S1** and **Table S1**). [25–27]

$$\frac{A_{0-0}}{A_{0-1}} \approx \left(\frac{1-0.24W/E_p}{1+0.073W/E_p}\right)^2 \quad (1)$$

The (0-0) and (0-1) vibronic peaks near the optical absorption edge are ascribed to the crystalline phase and the ratio of the two has been shown to correlate with W.[22] The value of W allows us to estimate the magnitude of interchain coupling in aggregates, where a decrease is indicative of an increase in conjugation length and aggregation in the film.[22] In our RR- and RRa-P3HT blend films, W is in a narrow range of 85 to 100 meV and shows no clear correlation with the amount of RR-P3HT, consistent with literature (**Figure 1(b)**). [28] For comparison, films of RR-P3HT cast from different solvents had an aggregate fraction between 0.33 to 0.46, but with a wide range of W, from 30 to 155meV.[17,22] In contrast, the blend films here have a narrow range of W, but a wide range of aggregate fraction. The value of W has shown correlation with charge transport,[17,29,30] therefore we expect that the ordered regions of the blend films should have comparable properties, but vary in number between the films.

Carrier concentration increases linearly with % RR- P3HT in blend through integer charge transfer. The optical spectra of films doped to saturation with F_4TCNQ from the vapor phase show that integer charge transfer occurs regardless of the composition of the blend **(Figure 1(c))**. The doped film of RR-P3HT shows bleaching of the neutral P3HT peak around 2.2eV, appearance of P3HT polaron peaks near 0.5 and 1.7eV, and F_4TCNQ anion peaks at 1.4 and 1.6eV. In the 100% RRa-P3HT film, there is a clear increase in intensity of the polaron and anion peaks, but the overlap

This article is protected by copyright. All rights reserved.

Author Manuscript

2199160x, 2019, 11, Downloaded from https://onlinelibrary.wiley.com/doi/10.1002/aelm.201800915, Wiley Online Library on [22/02/2024]. See the Terms and Conditions (https://onlinelibrary.wiley.com/terms-and-conditions) on Wiley Online Library for rules of use; OA articles are governed by the applicable Creative Commons License

of the spectral features above 2.7 eV makes it difficult to fit the spectra quantitatively. No spectral signature of a charge transfer complex was observed in the films.[31]

The optical transition of the polaron shows a gradual blue-shift from 0.46 to 0.64eV with decreasing percentage of RR-P3HT in the blend. A model for the spectra of doped P3HT based on a Holstein-style Hamiltonian suggests that as the distance between the counterion to the hole decreases, the energy of the polaron absorption increases.[32] Simulation of mid IR absorption for an oxidized P3HT aggregate with five 10-mer chains with various distances of dopant anion distance showed that this blue-shift is associated with the location of the F_4TCNQ anion relative to the polymer backbone.[18,33] This model suggests that the blend films with a higher fraction of RRa-P3HT have closer spacing between the dopant and the charge on the polymer backbone. Electron diffraction has shown that F_4TCNQ resides in the sidechains of crystallites of RR-P3HT in a regular fashion.[14] It is possible that the higher free volume in RRa-P3HT more easily accommodates dopant molecules in sites closer to the polymer backbone compared to semicrystalline RR-P3HT. An alternative possibility is that the films with higher RRa- fraction have chains with smaller conjugation lengths and more widely spaced electronic levels,[34,35] so the corresponding optical transition in the oxidized chains is larger.

The carrier concentration in the doped blend films was calculated from both absorbance and electron paramagnetic resonance (EPR) spectroscopies. [9,11,18,36] The absorbance spectra can be fit to find either the F_4TCNQ anion concentration, or the P3HT polaron concentration, to determine the number of carriers, which in turn can be used to calculate carrier concentration. Fitting the optical spectra to find the F_4TCNQ anion concentration is challenging for RR-:RRa- blends due to both the overlap of neutral and charged species of P3HT and F_4TCNQ peaks and the shift of peaks upon doping. However, values from fits of the F_4TCNQ anion have shown agreement with fits of the P3HT polaron [9] in vapor doped RR-P3HT films.[13] Thus, we calculated the carrier concentration as a function of %RR- P3HT by fitting the polaron and compared the results with the relative number of

This article is protected by copyright. All rights reserved.

Author Manuscript

2199160x, 2019, 11, Downloaded from https://onlinelibrary.wiley.com/doi/10.1002/aelm.201800915, Wiley Online Library on [22/02/2024]. See the Terms and Conditions (https://onlinelibrary.wiley.com/terms-and-conditions) on Wiley Online Library for rules of use; OA articles are governed by the applicable Creative Commons License

unpaired spins from EPR spectroscopy (**Figure S2**). Because P3HT films show structural anisotropy and EPR signal intensity is orientation dependent[37–39], determining the exact number of carriers in a film using EPR is challenging. Thus, the normalized EPR signal intensity was used to determine the relative amount of unpaired spins in doped films.

The concentration of charge carriers in films doped to saturation with F_4TCNQ increases linearly with the increasing fraction of RR-P3HT based on analysis of UV-Vis and EPR spectra. **Figure 2(a)** shows the calculated carrier concentration of doped films from the optical spectra and the normalized EPR signal intensity as a function of % RR-P3HT. The carrier concentrations of 100% RRa- and 100% RR- P3HT films were 0.3 x 10^{20} /cm^3 and 1.1 x 10^{20} / cm^3 respectively, and carrier concentrations of blends linearly increased with % RR-P3HT (**Table 1**). These values are in the same order of magnitude with values from sequentially doped RR-: RRa-P3HT blend films, where 10% RR- to 100% RR- P3HT films had carrier concentrations of 0.9 x 10^{20} /cm^3 to 4.0 x 10^{20} /cm^3.[18] Determining the precise carrier concentration from both measurement techniques possess inherent limitations. The absorption of the polaron peak around 0.5eV is assumed to be directly proportional to the amount of polaron in the film. However, the oscillator strengths of the P3HT polaron in different % RR- blends are unknown and could potentially vary. In EPR, the signal intensity is known to vary with orientation of the semicrystalline domains with respect to the applied magnetic field due to the anisotropy in lamellar stacking.[1–3] Despite the limitations in the two measurement techniques, relative changes in calculated carrier concentration from UV-vis and the normalized signal intensity from EPR as a function of % RR- P3HT are in good agreement.

The increase in carrier concentration with RR- content in the blend can be attributed to two factors. First, the larger ionization energy of RRa-P3HT should reduce the driving force for charge transfer and we expect that there will be fewer carriers as the disordered fraction increases. The doped pure RRa-P3HT film only has ~0.01 carrier/monomer. Second, F_4TCNQ is soluble in the disordered domains. Therefore, as the RRa-fraction increases, the dopants may be less likely to enter the semicrystalline regions and instead dope them at the boundaries between the ordered and disordered

This article is protected by copyright. All rights reserved.

Author Manuscript

2199160x, 2019, 11, Downloaded from https://onlinelibrary.wiley.com/doi/10.1002/aelm.201800915, Wiley Online Library on [22/02/2024]. See the Terms and Conditions (https://onlinelibrary.wiley.com/terms-and-conditions) on Wiley Online Library for rules of use; OA articles are governed by the applicable Creative Commons License

regions. The change in charge carrier concentration as a function of % RR-P3HT is likely due to contributions from both these effects, but it is difficult to quantitatively separate them.

Electrical conductivity and charge carrier mobility increase non-linearly with % RR- P3HT in vapor doped films. The doped films showed a nonlinear increase in conductivity with RR-P3HT content in contrast to the change in carrier concentration. The in-plane electrical conductivity of neat and 5% RRa- P3HT films were below the lower limit of our instrument (~10^{-7} S/cm) and unmeasurable. All other blend films had conductivities of ~10^{-5} S/cm in the neat state and showed no distinct trend as a function of RR- fraction **(Figure S3)**. The conductivity of doped RRa- P3HT film was 0.007 S/cm, 5% RR- P3HT was 0.37S/cm, films with 10 to 30 % RR- P3HT were around 1.5-2.5 S/cm, 50 % RR- P3HT was 7.3 S/cm, and 70 to 100% RR- P3HT were 10 to 15 S/cm (**Figure 2(b), Table 1**). The conductivity increased by over two orders of magnitude from 0 to 10% RR-P3HT, whereas the conductivity increased by only about tenfold from 10% to 100% RR-P3HT.

Because both carrier concentration and carrier mobility are influenced by degree of crystalline order and doping process, the knowledge of carrier concentration and mobility of films is important in order to understand observed behaviors in conductivity. The carrier mobilities of doped films were calculated from the electrical conductivity and carrier concentration and exhibit nonlinear behavior with % RR-P3HT. As seen in **Figure 2(c)**, the mobility increases rapidly from 0.00017 cm^2/Vs to 0.03 cm^2/Vs in 0 to 10% RR- P3HT, plateaus around 0.3 cm^2/Vs in 10-30% RR-P3HT, and increases to a second plateau around 0.8cm^2/Vs in 50% and higher RR-P3HT films. A similar trend is observed when plotted as a function of percentage of aggregates; the mobility increases sharply from 0 to 12% aggregates, exhibits a first plateau from 12 to 40%, and a second plateau from 40 to 56% aggregates (**Figure S4**). This nonlinear behavior is consistent with reported mobilities of RR-:RRa-P3HT films in gated transistors, where the field-effect mobility showed a sharp increase from 5 to 20% RR-P3HT

This article is protected by copyright. All rights reserved.

Author Manuscript

2199160x, 2019, 11, Downloaded from https://onlinelibrary.wiley.com/doi/10.1002/aelm.201800915, Wiley Online Library on [22/02/2024]. See the Terms and Conditions (https://onlinelibrary.wiley.com/terms-and-conditions) on Wiley Online Library for rules of use; OA articles are governed by the applicable Creative Commons License

and plateaued after 50% RR-P3HT (**Figure S5**).[28] The similarity of the behavior of the bulk conductivity and the behavior of the field-effect mobility from thin film transistors (TFTs) suggests that morphological changes with fraction of RR-P3HT are the origin of the differences in mobility with composition.

GIWAXS shows that vapor phase doping induces local ordering in the blend films. Grazing incidence wide angle X-ray scattering **(**GIWAXS) shows that the blending RR- and RRa-P3HT allows control over degree of order without changing the local structure of the crystalline regions (**Figure 3)**. The neat film of RRa-P3HT shows a broad background with no scattering peaks, indicating that the film is amorphous. Neat films of RR- and blends of RR-:RRa-P3HT show crystalline domains with a lamellar structure with edge-on texture. Changing the blend ratio has little effect on the structure and texture of the ordered domains, but the scattering intensity is stronger for films with higher % RR-P3HT, indicating that they more ordered domains (**Table S2, S3**). The correlation length of the crystallites based on the FWHM of the (100) peak is ≈15 nm for the blends with 50% or greater RR-P3HT, but significantly smaller for the dominantly RRa- blends with values of ≈ 5 nm (representing only a few molecular layers). The π stacking and alkyl stacking distances in the ordered domains in RR-P3HT are 3.83Å and 16.1Å respectively and are relatively insensitive to blending with RRa-P3HT. The alkyl stacking distances decrease slightly upon blending with RRa-P3HT and the (100) peak becomes broader until 90% RRa-P3HT, in which the alkyl stacking distance is 16.2 Å and the (200) and (300) reflections are absent.

Upon doping with F_4TCNQ, the RR-P3HT and blend films retain edge-on texture with a slight increase in alkyl stacking distance and a decrease π stacking distance compared to neat films consistent with previous results.[11,13] The peak locations and full-width at half maximum (FWHM) values are summarized in **Table S4-S6**. The correlation length of the crystallites based on the FWHM

This article is protected by copyright. All rights reserved.

Author Manuscript

2199160x, 2019, 11, Downloaded from https://onlinelibrary.wiley.com/doi/10.1002/aelm.201800915, Wiley Online Library on [22/02/2024]. See the Terms and Conditions (https://onlinelibrary.wiley.com/terms-and-conditions) on Wiley Online Library for rules of use; OA articles are governed by the applicable Creative Commons License

of the (100) for the doped blends with 50% or greater RR-P3HT is relatively unchanged from the neat films. In contrast, the dominantly RRa- blends have significantly more order than the neat films with larger correlation lengths of ≈9 nm. The peak near 1.62 $Å^{-1}$ has been previously observed in RR-P3HT doped with F_4TCNQ and emerges when dopants start to infiltrate the crystalline regions.[11] This peak is present in all blends and is less pronounced in doped RRa- films, consistent with a previous study.[13]

The emergence of diffraction peaks in upon doping the RRa-P3HT film indicates that dopant molecules act as additives that induce ordering in the film (**Figure 4**). Although the neat RRa-P3HT film has no scattering features other than a broad amorphous background and cannot form a true crystal due to the irregularity in the sidechain, the doped RRa-P3HT film shows scattering indicating alkyl and π stacking with crystallites with a lamellar, edge-on structure. The alkyl and π stacking distances of doped films of RRa-P3HT are 17.2 Å and 3.57 Å, and RR-P3HT are 17.8 Å and 3.63 Å. The observed texture and *d*-spacings are similar in doped RRa- and RR-P3HT films, suggesting that the RRa- polymer chains in neat films could be in a nematic-like arrangement prior to doping.[24] The polymer chains are likely preferably parallel to the substrate, but are disordered such that scattered waves cannot form constructive diffraction pattern in GIWAXS. This type of order may be comparable to that in the rigid-amorphous fractions (RAFs) of RR-P3HT; RAFs are disordered regions adjacent to crystalline domains that have partial ordering[40–42] Upon addition of F_4TCNQ, the charge transfer and formation of polarons increase the conjugation length, i.e. the planarity, as observed in Raman spectra.[18] This could induce long-range periodicity of polymer chains that would produce the observed diffraction pattern. Because the temperature of the P3HT film in doping chamber is above its T_g during vapor doping, rearrangement of polymer chains into crystallites is feasible but is not observed to occur without the dopant at comparable temperatures. The transition temperature for motion of the sidechains of RRa-P3HT is lower than for RR-P3HT,[43] which could also contribute to the structural rearrangement. The de-doped RRa-P3HT film shows no scattering

This article is protected by copyright. All rights reserved.

Author Manuscript

2199160x, 2019, 11, Downloaded from https://onlinelibrary.wiley.com/doi/10.1002/aelm.201800915, Wiley Online Library on [22/02/2024]. See the Terms and Conditions (https://onlinelibrary.wiley.com/terms-and-conditions) on Wiley Online Library for rules of use; OA articles are governed by the applicable Creative Commons License

peaks in GIWAXS (**Figure S6**), suggesting that it returns to its disordered state upon removal of dopants. This observation agrees with the absorbance spectra of doped and de-doped films that also shows vapor doping is a reversible process (**Figure S7**). This result also suggests that a fraction of the RRa- domains in the blended films likely crystallize as well, but it is difficult to separate the populations in the blend films due to the small separation of the *d*-spacing.

The in-plane scattering also reveals differences in the ordering of the RR- and RRa- domains. The secondary in-plane peak is observed in doped RR-P3HT, but disappears with films with higher % RRa- P3HT. In the unit cell of RR-P3HT, the lengths of *b* and *c* axis, that correspond to π-π stacking and thiophene backbone periodicity are very close to 7.8Å.[44] The neat RR-P3HT film and films has one distinguishable in-plane peak around 1.64Å^{-1} (3.83Å) which can have contributions from (020) π-π stacking and thiophene backbone periodicity that are very close to each other. In doped RR-P3HT film, there are two in-plane peaks at 1.62Å^{-1} (3.88Å) and 1.73Å^{-1} (3.63Å). The emergence of two peaks can arise due to decreased π-π stacking distance such that the peaks from the *b* and *c* axis become distinguishable. Recent electron diffraction studies of aligned doped films of P3HT are in agreement with this interpretation.[14] In the case of doped RRa-P3HT films, only one in-plane peak corresponding to π-π stacking is observed. The observation of one peak is reasonable considering the lack of long-range ordering of polymer backbone in RRa-P3HT film. Alternatively, it has also been suggested that the lower *q* peak is from some other periodicity in the co-crystalline phase of the polymer and the dopant.[45] It is difficult to completely rule out this possibility due to the small changes in the scattering pattern and lack of quantitative models of the structure, but the agreement with electron microscopy suggests the former interpretation.

Both alkyl- and π- stacking distances in doped films increase with RR-P3HT content, where 100% RRa- and RR-P3HT films have alkyl and π- stacking distances of (17.17Å, 3.57Å) and (17.80Å, 3.63Å) respectively, unlike neat films in which they were relatively insensitive to amount of RR-P3HT. The *d*-spacings of crystalline domains are slightly shorter in RRa- films than those of RR-

This article is protected by copyright. All rights reserved.

Author Manuscript

2199160x, 2019, 11, Downloaded from https://onlinelibrary.wiley.com/doi/10.1002/aelm.201800915, Wiley Online Library on [22/02/2024]. See the Terms and Conditions (https://onlinelibrary.wiley.com/terms-and-conditions) on Wiley Online Library for rules of use; OA articles are governed by the applicable Creative Commons License

P3HT despite the smaller apparent charge carrier density in the overall film from UV-Vis and EPR. The differences are therefore due to the sidechain structure rather than carrier concentration; the differences are sufficiently small that changes in the conformation of the disordered sidechains are the likely origin.

Raman spectroscopy shows stiffening of polymer backbone upon doping. Raman scattering was measured for all blend ratios of neat films to determine if there were local changes in the order of the polymer chains. **Figure 5** shows normalized Raman spectra of neat and doped RR- and RRa- films excited off-resonance (633nm) to gain information that is averaged over the entire film. Undoped RR-P3HT has two strong peaks centered at ~1380 cm^{-1} and ~1445 cm^{-1},which are assigned to the thiophene C-C bond stretch and the symmetric C=C bond stretch respectively[46]. RRa-P3HT has two peaks at 1378 cm^{-1}, 1393 cm^{-1}, and one peak at 1450 $cm^{-1.}$ The splitting of C-C peak into two is attributed to contributions from the tail-to-tail and head-to-head populations in the backbone.[47,48] The symmetric C=C bond stretching peak is significantly broader than that of RR-P3HT due to larger number of configurations and stretching modes, and the center of this peak is at higher wavenumber than that of RR-P3HT, which is consistent with previous studies.[47,48] Raman spectra of blend films of RR-:RRa- showed little difference from the spectra of RR-P3HT (**Figure S8**). In doped film of RR-P3HT and blends containing 10% or more RR-P3HT, the peaks at 1380cm^{-1} and 1445 cm^{-1} broaden and shift to lower energy (**Figure S8** and **S9**). The broadening after dopant incorporation is attributed to increase in number of polymer confirmations contributing to stretch modes.[49] The shift of the peaks to lower wavenumber is due to increase in coplanarity of the backbone, which in turn increases the delocalization of π electrons. A shoulder at 1325 cm^{-1} and a peak at 1420cm^{-1} emerged in doped films indicating presence of populations with longer conjugation length than neutral P3HT. This feature has been attributed to straightening of the polymer backbone at the amorphous/crystalline interface due to the interaction between polymer and dopant.[18] In vapor doped films of RRa-P3HT,

This article is protected by copyright. All rights reserved.

Author Manuscript

2199160x, 2019, 11, Downloaded from https://onlinelibrary.wiley.com/doi/10.1002/aelm.201800915, Wiley Online Library on [22/02/2024]. See the Terms and Conditions (https://onlinelibrary.wiley.com/terms-and-conditions) on Wiley Online Library for rules of use; OA articles are governed by the applicable Creative Commons License

we observe that symmetric C=C bond stretching peak around 1450cm^{-1} becomes narrower and moves closer to the C=C peak in undoped RR-P3HT. Based on these data, stiffening of polymer backbone in amorphous regions should lead to a longer conjugation length aiding charge transport.

RSoXS shows the dominant OCL in doped film is correlated with carrier mobility Resonant soft X-ray scattering (RSoXS) was used to study long-range connectivity of domains in P3HT films. The 1s to π* transition dipole moment of P3HT points perpendicular to the plane of the thiophene rings. Thus, by tuning the incident polarized *X*-ray to the 1s to π* resonance energy, we can achieve scattering contrast from the conjugated backbone and obtain information about the length scale of the alignment of ordered domains.[10,13,15,50] The orientation correlation length (OCL) is a measure of the length scale over which domains with aggregated polymer backbones are aligned with neighboring backbones, which has shown to be correlated with charge mobility and conductivity in semiconducting polymers.[33,34] In the blend samples, the ordered P3HT domains are highly textured in an edge-on orientation and the 1s→π* transition will make a strong contribution to the scattering.[13,30] The domains with disordered P3HT chains will not have transitions that are as well-aligned with the incident beam and will have weaker scattering.

RSoXS profiles of neat blend films show three distinct regimes with varying % RR-P3HT (**Figure 6(a)**); where i) there is no observable feature in the scattering, ii) the scattering is dominated by a shorter OCL, and iii) scattering is dominated by a longer OCL. There are no clear peaks observed in the 0% and 30% RR-P3HT blend films suggesting no correlation between domains. This is expected for amorphous P3HT and suggests that there is no strong correlation between the ordered domains in the 30% blend. In the other compositions, peaks for a shorter and a longer OCL are observed near q=0.035Å^{-1} (OCL = 9 nm) and q=0.015Å^{-1} (OCL = 21nm) respectively. The intensity of

This article is protected by copyright. All rights reserved.

Author Manuscript

2199160x, 2019, 11, Downloaded from https://onlinelibrary.wiley.com/doi/10.1002/aelm.201800915, Wiley Online Library on [22/02/2024]. See the Terms and Conditions (https://onlinelibrary.wiley.com/terms-and-conditions) on Wiley Online Library for rules of use; OA articles are governed by the applicable Creative Commons License

the peak at higher q initially dominates until 70 % RR-P3HT, where the relative intensity of lower q peak increases.

Doping results in an increase in the correlation length of the domains for all blend films, evidenced by the emergence and increase in scattering intensity of both the short and long OCL. In doped films, 0% RR- has a peak at 0.034Å^{-1} (9.2nm) while 30% RR- film has both low and high q peaks at 0.018 Å^{-1} (17nm) and 0.034Å^{-1} (9.2nm) (**Figure 6(b)**). In the doped RRa-P3HT film, there is a peak at 0.034Å^{-1} (9.2nm), consistent with GIWAXS and Raman results showing induced crystallization from doping. While the ordering within crystalline domains of the doped RRa- film is similar to that of the doped RR-P3HT film, the longer-range correlation between crystalline regions of the doped RRa- film is smaller. The lack of correlation between domains occurs because there are a smaller number of crystalline domains in the doped RRa- film, confirmed by the relative peak heights in respective GIWAXS patterns, that are sparsely distributed throughout the film. In 30% RR- blend film, although the undoped film has crystalline domains, RSoXS showed no peak in this q-range potentially due to a peak being at higher q (OCL smaller than 10 nm), or the film has a low density of orientationally correlated domains. Upon doping the 30% RR- blend film, we interpret emergence of two scattering peaks as contributions from the amorphous regions, the short OCL (9.2 nm), and the crystalline regions, the longer OCL (17 nm). Doped films of blends films with higher % RR-P3HT have both low and high q peaks, with low q peak shifted to higher q and high q peak roughly unchanged from the undoped state. While the origin of the small decrease in OCL from the low q peak upon doping still needs to be further investigated, this shows that both the crystalline and amorphous regions go through morphological changes from doping from the chain stiffening observed by Raman spectroscopy.

The lack of a longer OCL of the domains in RRa-P3HT film, which was present in blends with higher RR content, rationalizes the low carrier mobility. The sharp increase in mobility from 30% RR- to 70% RR correlates well with the relative density of domains that correspond to the higher OCL peak observed in RSoXS profiles (**Figure 6c**). While domains with smaller OCL contribute to charge

This article is protected by copyright. All rights reserved.

Author Manuscript

2199160x, 2019, 11, Downloaded from https://onlinelibrary.wiley.com/doi/10.1002/aelm.201800915, Wiley Online Library on [22/02/2024]. See the Terms and Conditions (https://onlinelibrary.wiley.com/terms-and-conditions) on Wiley Online Library for rules of use; OA articles are governed by the applicable Creative Commons License

transport as seen in RRa-P3HT film, transport through domains with longer OCL is more efficient; it provides longer percolated path way for charge carriers to travel, thereby significantly increasing the carrier mobility in the film. There likely exists a threshold concentration of the higher OCL population above which increase in the amount of higher OCL population has little effect on charge transport, which occurs in the 50 to 70% RR-P3HT films.

Impact of blending on thermoelectric properties. The viability of thermoelectric materials is assessed by their figure of merit, *ZT*, Eq. 2 where *S* is Seebeck coefficient, σ is electrical conductivity, and κ is thermal conductivity at a given temperature T.

$$ZT = \frac{S^2 \sigma T}{\kappa} \qquad (2)$$

This relationship shows that the figure of merit can be maximized by increasing the power factor $S^2\,\sigma$ (PF), or minimizing thermal conductivity. The Seebeck coefficient of a semiconductor is related to the shape of density of states and states occupied by charge carriers near Fermi energies and scattering processes.[6,51] Due to the anisotropic nature of charge transport in conjugated polymers and the interplay of charge transfer and change in morphology upon doping, predicting the thermopower of a doped semiconductor film is challenging.[52] Because the electrical conductivity can vary considerably as a function of crystallinity of the film at similar levels of doping, it is important to assess its effect on the Seebeck coefficient and also the power factor.

The Seebeck coefficient in vapor-doped P3HT blend films is not strongly impacted by morphology and shows a correlation with carrier concentration. Doped films of 5% RR- and 100% RR- P3HT films have Seebeck coefficients of 121 $\pm$ 10 μV/K and 77 $\pm$ 8 μV/K, with carrier concentrations of 0.3×10^{20} and 1.1×10^{20} /cm^3 respectively. The Seebeck coefficient is in the range of 66 to 110 μV/K for the RR-:RRa- P3HT blends **(Table S7)**. The decrease in Seebeck coefficient with increasing RR-P3HT content in films can be explained by the higher carrier concentration in

This article is protected by copyright. All rights reserved.

Author Manuscript

2199160x, 2019, 11, Downloaded from https://onlinelibrary.wiley.com/doi/10.1002/aelm.201800915, Wiley Online Library on [22/02/2024]. See the Terms and Conditions (https://onlinelibrary.wiley.com/terms-and-conditions) on Wiley Online Library for rules of use; OA articles are governed by the applicable Creative Commons License

crystalline films. Previously, it was shown that long-range correlation in PBTTT films has strong impact on electrical conductivity while Seebeck coefficient does not substantial changes.[10] Our result is complimentary to the previously study showing that Seebeck coefficient has a weaker trend with the composition of the blend than the electrical conductivity. The power factor in vapor doped films of RR-: RRa-P3HT blend is governed by morphology because of the stronger impact on of composition on the electrical conductivity. The power factors of doped 5% RR- and 100% RR-P3HT films are 0.45μW/mK^2 and 8.0μW/mK^2. The power factor increased with increasing % RR- P3HT due to the better long-range connectivity that led to higher charge mobility and conductivity in these films (**Figure S10**).

The thermoelectric performance of polymer blend films rely on the interplay of a number of factors that rely on the morphology of the blend. The energetic driving force for charge transfer with a dopant of the polymers and the miscibility of the major and minor components can both impact the Seebeck and electrical conductivity. It has been suggested that blending RR-P3HT with a minor (~2%) additive component with a lower ionization energy, such as poly(3-hexylthiothiophene), P3HTT ($\Delta IE_{\text{P3HT-PHTTT}}$ ≈0.15eV), is a route for designing thermoelectric materials to simultaneously increase Seebeck coefficient and electrical conductivity.[53] Blends of a minor component (5-10%) of RR-P3HT and major component with deeper HOMO level, such as the thieno[3,4-b]-thiophene-co-benzodithiophene polymer PTB7 ($\Delta IE_{\text{PTB7-P3HT}}$ ≈0.33eV) and the quinoxaline-thiophene copolymer TQ1($\Delta IE_{\text{TQ1-P3HT}}$ ≈0.46eV, also showed a significant increase in Seebeck coefficient while preserving reasonable electrical conductivities.[54] It was suggested that by doping the composite material, charge transport will occur from the charge carriers near the Fermi level of the major component, while the minor component creates occupied states farther away from the Fermi level, thereby increasing the Seebeck coefficient. [53] [54] In our blend films, this is equivalent to having RRa-P3HT as the major component and RR-P3HT as minor component because the ionization energy of RRa-P3HT thin film is lower than that of RR-P3HT ($\Delta IE_{\text{RR–RRa}}$ ≈ 0.25 eV).[34,35]. Our results address the

This article is protected by copyright. All rights reserved.

Author Manuscript

2199160x, 2019, 11, Downloaded from https://onlinelibrary.wiley.com/doi/10.1002/aelm.201800915, Wiley Online Library on [22/02/2024]. See the Terms and Conditions (https://onlinelibrary.wiley.com/terms-and-conditions) on Wiley Online Library for rules of use; OA articles are governed by the applicable Creative Commons License

question of the role of morphology and phase separation that have been previously raised in the limit of a well-mixed system.[55] We see a decrease in the Seebeck coefficient and large increase in conductivity with increasing concentration of RR-P3HT. We believe that the large increase in conductivity is due to the increased order and connectivity of the ordered domains due to addition of the minor component, RR-P3HT. At larger loadings of RR-P3HT, the Seebeck coefficient drops at 50% and stays at a comparable value within error while the electrical conductivity continues to increase in agreement with RSoXS that suggests better connectivity of the order domains that should dominate the electrical properties (**Table S6**). It is difficult to disaggregate the contributions of the two domains due to their differing doping efficiencies suggesting that future studies to better engineering of Seebeck coefficient and electrical conductivity in blends would benefit from independent control of the doping in both phases.

We can also compare our results with an empirical trend for the relationship observed between the Seebeck coefficient and the electrical conductivity for numerous doped organic semiconductors. The two properties tend to follow a power law relationship that is the subject of theoretical modeling.[8] **Figure 7(a) and 7(b)** shows Seebeck coefficient and power factor as a function of conductivity in this study and reported empirical trends ($S \propto \sigma^{-\frac{1}{4}}$, $PF \propto \sigma^{\frac{1}{2}}$).[10] The Seebeck coefficient is a function of charge carrier concentration near the Fermi level of semiconducting polymer, and has shown to be relatively independent of connectivity between domains. On the other hand, the conductivity depends on both the carrier concentration and charge mobility, which depends on morphology of film. While our results follow the general trend of increasing Seebeck and decreasing power factor as a function of conductivity, it deviates from the empirical trend due to changes in morphology in the blends. Compared to this power-law relationship, the change in Seebeck of 77 μV/K to 110 μV/K in our vapor doped RR-: RRa-P3HT films is minimal for the the change in conductivity from 0.37 S/cm to 13.4 S/cm. The relatively similar carrier concentrations in the blend films led to narrow range of Seebeck coefficients, but with varying

This article is protected by copyright. All rights reserved.

Author Manuscript

2199160x, 2019, 11, Downloaded from https://onlinelibrary.wiley.com/doi/10.1002/aelm.201800915, Wiley Online Library on [22/02/2024]. See the Terms and Conditions (https://onlinelibrary.wiley.com/terms-and-conditions) on Wiley Online Library for rules of use; OA articles are governed by the applicable Creative Commons License

conductivity largely due to the differences in the connectivity of domains. We compare our data with the empirical trend, $S = \frac{k_B}{e}(\frac{\sigma}{\sigma_0})^{-\frac{1}{4}}$, where $\frac{k_B}{e}$ is the natural unit of thermopower, 86.17 μV/K and σ_0 is a pre-factor set at a value of 1 S/cm.[56] The data for the blend films is shifted to the right compared to the empirical trend due to higher conductivity at a given carrier concentration because of the higher carrier mobility. For a given Seebeck value, the difference in measured conductivity and the expected conductivity from the empirical trend increased with % RR P3HT. This difference corresponds to a change in the pre-factor and has been suggested in transport models as a route to improve the thermoelectric performance of polymers.[57] For a given conductivity value, the difference in the measured and the expected PF from the empirical trend, δ, increased with % RR P3HT, ranging from δ≈-0.04 μW/mK^2 in 5% RR- to ≈ 5μW/mK^2 in 100% RR-P3HT film. Vapor doped films with higher % RR- P3HT sits further above this empirical trend line than lower % RR-P3HT films due to better doping efficiency and connectivity of domains for charge transport.

Because of the heterogeneous nature of semicrystalline polymers, consisting of ordered and disordered regions that affect charge transport, it is important to consider the form of the electronic density of states (DOS) to interpret differences in thermoelectric properties. Current models for thermoelectric properties assume a homogeneous electronic DOS for modelling transport in organic semiconductors.[58–62] However, semiconducting polymers that form both amorphous and crystalline regions in solid state cannot be accurately represented by a single DOS model. For example, if the dopants preferentially reside in the amorphous regions,[63] the film could have amorphous regions with high carrier density and crystalline regions with low carrier density. In the amorphous regions, carriers would occupy states near the Fermi level for hopping, but could have difficulty finding mobile states to hop to in the ordered regions. Thus, both the knowledge of morphology of the film, location of the dopants, and an appropriate DOS model to account for the heterogeneity in electronic states are crucial in understanding and predicting charge transport in doped films.

This article is protected by copyright. All rights reserved.

Author Manuscript

2199160x, 2019, 11, Downloaded from https://onlinelibrary.wiley.com/doi/10.1002/aelm.201800915, Wiley Online Library on [22/02/2024]. See the Terms and Conditions (https://onlinelibrary.wiley.com/terms-and-conditions) on Wiley Online Library for rules of use; OA articles are governed by the applicable Creative Commons License

Conclusion

We have revealed the role of ordering and morphology on the thermoelectric properties of doped P3HT by using a vapor-doping method. Casting blends of RR- and RRa-P3HT provided good control of the fraction of aggregates without altering their interchain order, conjugation length, and texture. Introduction of F_4TCNQ from the vapor-phase provided a route to study the electrical properties of these films with controlled morphologies. A surprising observation was crystallinity induced by doping in the RRa-P3HT phase with preferred texture and *d*-spacings. The connectivity of the ordered domains was revealed by RSoXS; films with higher crystallinity have better long-range connectivity between the domains and therefore better charge transport. Crystalline regions have a high doping efficiency than the amorphous regions due to energetic driving force for charge transfer. Thus, the electrical conductivity of heavily doped films increased with fraction of RR-P3HT due to interplay of higher carrier concentration from better doping efficiency and higher mobility from better long-range connectivity between the domains for charge transport. The Seebeck coefficient was not as strongly dependent on morphology as the electrical conductivity. In addition, there is a threshold concentration of crystalline regions and overall connectivity of films, above which the increase in conductivity and power factor is marginal. For this system without strong phase separation, the use of blend therefore does not lead to an improvement in power factor. These results provide a model system for understanding blends of polymers with varying ionization energy in thermoelectrics where phase separation plays an important role in their behavior.[55,64]

Acknowledgement

This work was supported by NSF DMR 1808622. E.L. received support from a National Science Foundation Graduate Research Fellowships (DGE-1144085). R.M. acknowledges support from the University of California LEADS program. Portions of the research were carried out at the Advanced

This article is protected by copyright. All rights reserved.

Author Manuscript

2199160x, 2019, 11, Downloaded from https://onlinelibrary.wiley.com/doi/10.1002/aelm.201800915, Wiley Online Library on [22/02/2024]. See the Terms and Conditions (https://onlinelibrary.wiley.com/terms-and-conditions) on Wiley Online Library for rules of use; OA articles are governed by the applicable Creative Commons License

Light Source, supported by the Director, Office of Science, Office of Basic Energy Sciences, of the U.S. Department of Energy under Contract No. DEAC02-05CH11231. The research reported here made use of shared facilities of the UCSB MRSEC (NSF DMR 1720256), a member of the Materials Research Facilities Network (www.mrfn.org). The authors would like to thank Dr. Alexander Mikhailovsky for technical assistance with Raman spectroscopy measurements and Saejin Oh for help with the GPC data.

References

[1] G.-H. Kim, L. Shao, K. Zhang, K. P. Pipe, *Nat Mater* **2013**, *12*, 719.

[2] R. A. Schlitz, F. G. Brunetti, A. M. Glaudell, P. L. Miller, M. A. Brady, C. J. Takacs, C. J. Hawker, M. L. Chabinyc, *Advanced Materials* **2014**, *26*, 2825.

[3] K.-H. Yim, G. L. Whiting, C. E. Murphy, J. J. M. Halls, J. H. Burroughes, R. H. Friend, J.-S. Kim, *Adv. Mater.* **2008**, *20*, 3319.

[4] B. Russ, M. J. Robb, F. G. Brunetti, P. L. Miller, E. E. Perry, S. N. Patel, V. Ho, W. B. Chang, J. J. Urban, M. L. Chabinyc, C. J. Hawker, R. A. Segalman, *Advanced Materials* **2014**, *26*, 3473.

[5] I. E. Jacobs, A. J. Moulé, *Advanced Materials* **2017**, 1703063:1.

[6] D. Venkateshvaran, M. Nikolka, A. Sadhanala, V. Lemaur, M. Zelazny, M. Kepa, M. Hurhangee, A. J. Kronemeijer, V. Pecunia, I. Nasrallah, I. Romanov, K. Broch, I. McCulloch, D. Emin, Y. Olivier, J. Cornil, D. Beljonne, H. Sirringhaus, *Nature* **2014**, *515*, nature13854.

[7] B. Russ, A. Glaudell, J. J. Urban, M. L. Chabinyc, R. A. Segalman, *Nature Reviews Materials* **2016**, *1*, 1.

[8] A. M. Glaudell, J. E. Cochran, S. N. Patel, M. L. Chabinyc, *Adv. Energy Mater.* **2015**, *5*, n/a.

[9] I. E. Jacobs, E. W. Aasen, J. L. Oliveira, T. N. Fonseca, J. D. Roehling, J. Li, G. Zhang, M. P. Augustine, M. Mascal, A. J. Moulé, *J. Mater. Chem. C* **2016**, *4*, 3454.

[10] S. N. Patel, A. M. Glaudell, K. A. Peterson, E. M. Thomas, K. A. O'Hara, E. Lim, M. L. Chabinyc, *Science Advances* **2017**, *3*, e1700434.

[11] D. T. Scholes, S. A. Hawks, P. Y. Yee, H. Wu, J. R. Lindemuth, S. H. Tolbert, B. J. Schwartz, *J. Phys. Chem. Lett.* **2015**, *6*, 4786.

[12] K. Kang, S. Watanabe, K. Broch, A. Sepe, A. Brown, I. Nasrallah, M. Nikolka, Z. Fei, M. Heeney, D. Matsumoto, K. Marumoto, H. Tanaka, S. Kuroda, H. Sirringhaus, *Nat Mater* **2016**, *15*, 896.

This article is protected by copyright. All rights reserved.

Author Manuscript

2199160x, 2019, 11, Downloaded from https://onlinelibrary.wiley.com/doi/10.1002/aelm.201800915, Wiley Online Library on [22/02/2024]. See the Terms and Conditions (https://onlinelibrary.wiley.com/terms-and-conditions) on Wiley Online Library for rules of use; OA articles are governed by the applicable Creative Commons License

[13] E. Lim, K. A. Peterson, G. M. Su, M. L. Chabinyc, *Chem. Mater.* **2018**, *30*, 998.

[14] A. Hamidi-Sakr, L. Biniek, J.-L. Bantignies, D. Maurin, L. Herrmann, N. Leclerc, P. Lévêque, V. Vijayakumar, N. Zimmermann, M. Brinkmann, *Adv. Funct. Mater.* **2017**, n/a.

[15] B. A. Collins, J. E. Cochran, H. Yan, E. Gann, C. Hub, R. Fink, C. Wang, T. Schuettfort, C. R. McNeill, M. L. Chabinyc, H. Ade, *Nat Mater* **2012**, *11*, 536.

[16] R. Noriega, J. Rivnay, K. Vandewal, F. P. V. Koch, N. Stingelin, P. Smith, M. F. Toney, A. Salleo, *Nature Materials* **2013**, *12*, 1038.

[17] J. Hynynen, D. Kiefer, C. Müller, *RSC Adv.* **2018**, *8*, 1593.

[18] A. R. Chew, R. Ghosh, Z. Shang, F. C. Spano, A. Salleo, *J. Phys. Chem. Lett.* **2017**, *8*, 4974.

[19] J. Clark, C. Silva, R. H. Friend, F. C. Spano, *Phys. Rev. Lett.* **2007**, *98*, 206406.

[20] P. J. Brown, D. S. Thomas, A. Köhler, J. S. Wilson, J.-S. Kim, C. M. Ramsdale, H. Sirringhaus, R. H. Friend, *Phys. Rev. B* **2003**, *67*, 064203.

[21] S. Nam, S. Lee, I. Lee, M. Shin, H. Kim, Y. Kim, *Nanoscale* **2011**, *3*, 4261.

[22] J. Clark, J.-F. Chang, F. C. Spano, R. H. Friend, C. Silva, *Applied Physics Letters* **2009**, *94*, 163306.

[23] C. R. Snyder, R. C. Nieuwendaal, D. M. DeLongchamp, C. K. Luscombe, P. Sista, S. D. Boyd, *Macromolecules* **2014**, *47*, 3942.

[24] X. Shen, W. Hu, T. P. Russell, *Macromolecules* **2016**, *49*, 4501.

[25] F. C. Spano, *Chemical Physics* **2006**, *325*, 22.

[26] F. C. Spano, *The Journal of Chemical Physics* **2005**, *122*, 234701.

[27] J. Clark, J.-F. Chang, F. C. Spano, R. H. Friend, C. Silva, *Applied Physics Letters* **2009**, *94*, 163306.

[28] P.-H. Chu, G. Wang, B. Fu, D. Choi, J. O. Park, M. Srinivasarao, E. Reichmanis, *Advanced Electronic Materials* **2016**, *2*, 1500384.

[29] J. Clark, J.-F. Chang, F. C. Spano, R. H. Friend, C. Silva, *Appl. Phys. Lett.* **2009**, *94*, 163306.

[30] K. Vakhshouri, B. H. Smith, E. P. Chan, C. Wang, A. Salleo, C. Wang, A. Hexemer, E. D. Gomez, *Macromolecules* **2016**, *49*, 7359.

[31] H. Méndez, G. Heimel, S. Winkler, J. Frisch, A. Opitz, K. Sauer, B. Wegner, M. Oehzelt, C. Röthel, S. Duhm, D. Többens, N. Koch, I. Salzmann, *Nature Communications* **2015**, *6*, 8560.

[32] R. Ghosh, C. M. Pochas, F. C. Spano, *The Journal of Physical Chemistry C* **2016**, *120*, 11394.

This article is protected by copyright. All rights reserved.

Author Manuscript

2199160x, 2019, 11, Downloaded from https://onlinelibrary.wiley.com/doi/10.1002/aelm.201800915, Wiley Online Library on [22/02/2024]. See the Terms and Conditions (https://onlinelibrary.wiley.com/terms-and-conditions) on Wiley Online Library for rules of use; OA articles are governed by the applicable Creative Commons License

[33] R. Ghosh, A. R. Chew, J. Onorato, V. Pakhnyuk, C. K. Luscombe, A. Salleo, F. C. Spano, *J. Phys. Chem. C* **2018**, *122*, 18048.

[34] W. C. Tsoi, S. J. Spencer, L. Yang, A. M. Ballantyne, P. G. Nicholson, A. Turnbull, A. G. Shard, C. E. Murphy, D. D. C. Bradley, J. Nelson, J.-S. Kim, *Macromolecules* **2011**, *44*, 2944.

[35] S. Ko, E. T. Hoke, L. Pandey, S. Hong, R. Mondal, C. Risko, Y. Yi, R. Noriega, M. D. McGehee, J.-L. Brédas, A. Salleo, Z. Bao, *J. Am. Chem. Soc.* **2012**, *134*, 5222.

[36] J. Gao, E. T. Niles, J. K. Grey, *The Journal of Physical Chemistry Letters* **2013**, *4*, 2953.

[37] H. Käss, P. Fromme, H. T. Witt, W. Lubitz, *J. Phys. Chem. B* **2001**, *105*, 1225.

[38] O. Gonen, H. Levanon, *J. Phys. Chem.* **1985**, *89*, 1637.

[39] D. W. Breiby, S. Sato, E. J. Samuelsen, K. Mizoguchi, *Journal of Polymer Science Part B: Polymer Physics* **2003**, *41*, 3011.

[40] D. C. Martin, J. Chen, J. Yang, L. F. Drummy, C. Kübel, *Journal of Polymer Science Part B: Polymer Physics* **n.d.**, *43*, 1749.

[41] B. Wunderlich, *Progress in Polymer Science* **2003**, *28*, 383.

[42] B. Wunderlich, *Journal of Macromolecular Science, Part B* **2003**, *42*, 579.

[43] R. Xie, Y. Lee, M. P. Aplan, N. J. Caggiano, C. Müller, R. H. Colby, E. D. Gomez, *Macromolecules* **2017**, *50*, 5146.

[44] N. Kayunkid, S. Uttiya, M. Brinkmann, *Macromolecules* **2010**, *43*, 4961.

[45] D. T. Scholes, P. Y. Yee, J. R. Lindemuth, H. Kang, J. Onorato, R. Ghosh, C. K. Luscombe, F. C. Spano, S. H. Tolbert, B. J. Schwartz, *Advanced Functional Materials* **2017**, *27*, 1702654.

[46] G. Louarn, M. Trznadel, J. P. Buisson, J. Laska, A. Pron, M. Lapkowski, S. Lefrant, *The Journal of Physical Chemistry* **1996**, *100*, 12532.

[47] S. Wood, J. R. Hollis, J.-S. Kim, *J. Phys. D: Appl. Phys.* **2017**, *50*, 073001.

[48] W. C. Tsoi, D. T. James, J. S. Kim, P. G. Nicholson, C. E. Murphy, D. D. C. Bradley, J. Nelson, J.-S. Kim, *J. Am. Chem. Soc.* **2011**, *133*, 9834.

[49] J. Gao, J. D. Roehling, Y. Li, H. Guo, A. J. Moulé, J. K. Grey, *J. Mater. Chem. C* **2013**, *1*, 5638.

[50] J. Rivnay, S. Inal, B. A. Collins, M. Sessolo, E. Stavrinidou, X. Strakosas, C. Tassone, D. M. Delongchamp, G. G. Malliaras, *Nature Communications* **2016**, *7*, 11287.

[51] Y. Xuan, X. Liu, S. Desbief, P. Leclère, M. Fahlman, R. Lazzaroni, M. Berggren, J. Cornil, D. Emin, X. Crispin, *Phys. Rev. B* **2010**, *82*, 115454.

This article is protected by copyright. All rights reserved.

Author Manuscript

2199160x, 2019, 11, Downloaded from https://onlinelibrary.wiley.com/doi/10.1002/aelm.201800915, Wiley Online Library on [22/02/2024]. See the Terms and Conditions (https://onlinelibrary.wiley.com/terms-and-conditions) on Wiley Online Library for rules of use; OA articles are governed by the applicable Creative Commons License

[52] R. Kroon, D. A. Mengistie, D. Kiefer, J. Hynynen, J. D. Ryan, L. Yu, C. Müller, *Chem. Soc. Rev.* **2016**, *45*, 6147.

[53] J. Sun, M.-L. Yeh, B. J. Jung, B. Zhang, J. Feser, A. Majumdar, H. E. Katz, *Macromolecules* **2010**, *43*, 2897.

[54] G. Zuo, X. Liu, M. Fahlman, M. Kemerink, *Advanced Functional Materials* **2018**, *28*, 1703280.

[55] G. Zuo, X. Liu, M. Fahlman, M. Kemerink, *ACS Appl. Mater. Interfaces* **2018**, *10*, 9638.

[56] A. M. Glaudell, J. E. Cochran, S. N. Patel, M. L. Chabinyc, *Adv. Energy Mater.* **2015**, *5*, n/a.

[57] S. D. Kang, G. J. Snyder, *Nat Mater* **2017**, *16*, 252.

[58] G. Kim, K. P. Pipe, *Phys. Rev. B* **2012**, *86*, 085208.

[59] D. Mendels, N. Tessler, *J. Phys. Chem. Lett.* **2014**, *5*, 3247.

[60] D. Wang, W. Shi, J. Chen, J. Xi, Z. Shuai, *Physical Chemistry Chemical Physics* **2012**, *14*, 16505.

[61] S. D. Kang, G. J. Snyder, *Nat Mater* **2017**, *16*, 252.

[62] N. Tessler, Y. Preezant, N. Rappaport, Y. Roichman, *Advanced Materials* **2009**, *21*, 2741.

[63] E. M. Thomas, M. A. Brady, H. Nakayama, B. C. Popere, R. A. Segalman, M. L. Chabinyc, *Advanced Functional Materials* **2018**, *28*, 1803687.

[64] H. E. Katz, T. O. Poehler, Eds. , *Innovative Thermoelectric Materials: Polymer, Nanostructure and Composite Thermoelectrics*, Imperial College Press, London, **2016**.

[65] E. Lim, K. A. Peterson, G. M. Su, M. L. Chabinyc, *Chem. Mater.* **2018**, *30*, 998.

Author Manuscript

This article is protected by copyright. All rights reserved.

2199160x, 2019, 11, Downloaded from https://onlinelibrary.wiley.com/doi/10.1002/aelm.201800915, Wiley Online Library on [22/02/2024]. See the Terms and Conditions (https://onlinelibrary.wiley.com/terms-and-conditions) on Wiley Online Library for rules of use; OA articles are governed by the applicable Creative Commons License

Author Manuscript

Figures

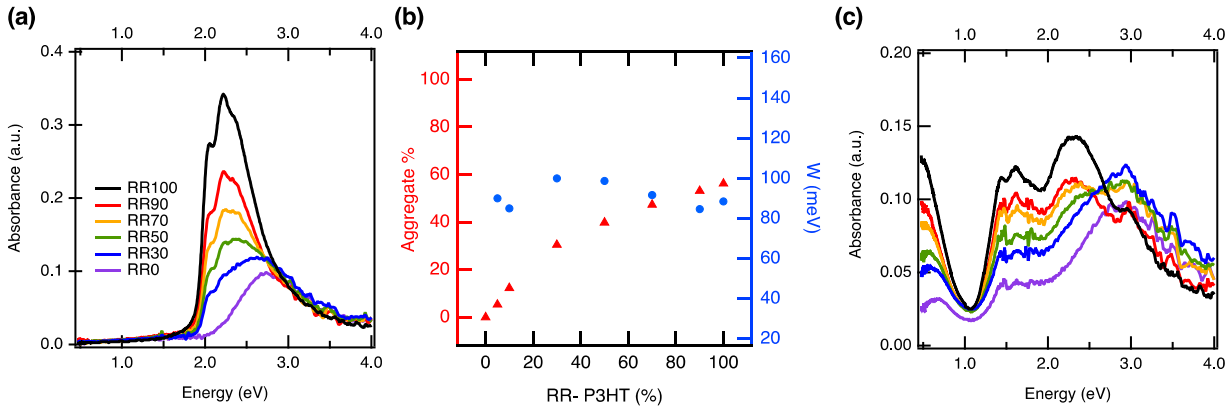

Figure 1. (a) UV-vis absorption spectra of neatRR-:RRa- P3HT blend films (b) free exciton bandwidth, W and aggregate fraction of neat films calculated from Spano model and (c) UV-vis absorption specra of vapor doped RR-:RRa- P3HT blend films.

This article is protected by copyright. All rights reserved.

2199160x, 2019, 11, Downloaded from https://onlinelibrary.wiley.com/doi/10.1002/aelm.201800915, Wiley Online Library on [22/02/2024]. See the Terms and Conditions (https://onlinelibrary.wiley.com/terms-and-conditions) on Wiley Online Library for rules of use; OA articles are governed by the applicable Creative Commons License

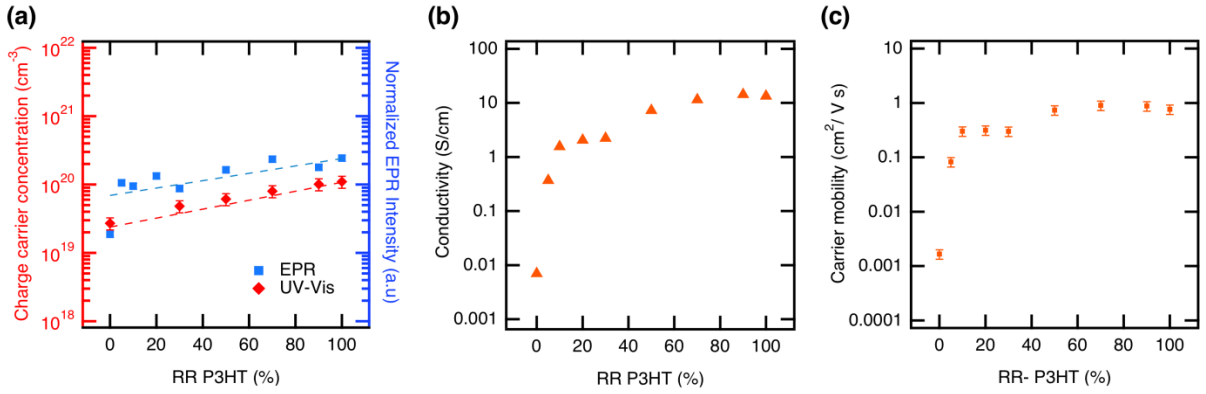

Figure 2. (a) Carrier concentration calculated from UV-Vis spectra and the normalized signal from EPR in arbitrary units. Both characterizations show that carrier concentration increases with % RR P3HT **(b)** Electrical conductivity of doped RR-:RRa- P3HT blend films as a function of % regioregular P3HT in blend; the conductivity of neat RRa-P3HT was unmeasurable (below 10^{-7} S/cm). **(c)** Carrier mobility of doped films versus carrier concentration calculated by UV-Vis absorption spectra.

Author Manuscript

This article is protected by copyright. All rights reserved.

2199160x, 2019, 11, Downloaded from https://onlinelibrary.wiley.com/doi/10.1002/aelm.201800915, Wiley Online Library on [22/02/2024]. See the Terms and Conditions (https://onlinelibrary.wiley.com/terms-and-conditions) on Wiley Online Library for rules of use; OA articles are governed by the applicable Creative Commons License

Table 1. Electrical conductivity of RR- : RRa-P3HT blend films saturation doped with F_4TCNQ

% RR P3HT	Electrical conductivity (S/cm)	Estimated Carrier Concentration (cm^{-3})
0	0.007	2.6×10^{19}
5	0.4	2.8×10^{19}
10	1.6	3.2×10^{19}
20	2.1	4.1×10^{19}
30	2.3	4.6×10^{19}
50	7.3	6.2×10^{19}
70	11.5	7.9×10^{19}
90	14.3	10×10^{19}
100	13.4	11×10^{19}

Author Manuscript

This article is protected by copyright. All rights reserved.

2199160x, 2019, 11, Downloaded from https://onlinelibrary.wiley.com/doi/10.1002/aelm.201800915, Wiley Online Library on [22/02/2024]. See the Terms and Conditions (https://onlinelibrary.wiley.com/terms-and-conditions) on Wiley Online Library for rules of use; OA articles are governed by the applicable Creative Commons License

Author Manuscript

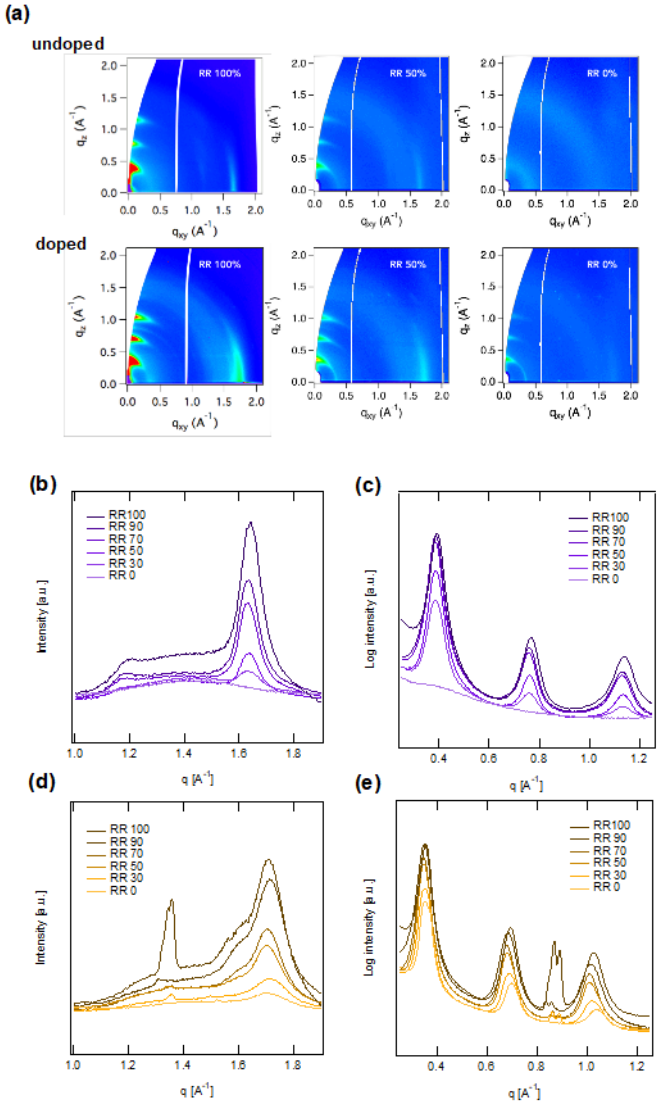

Figure 3. **(a)** 2D GIWAXS images of neat (top row) and doped (bottom row) RR-: RRa-P3HT blend films. Lincuts from these images are given in **(b)** undoped in-plane direction, **(c)** undoped out-of-plane direction near the inaccessible region, **(d)** doped in-plane direction and, **(e)** doped out-of-plane direction near the inaccessible region. High intensity peaks in (d) at 1.3 $Å^{-1}$ and (e) 0.85$Å^{-1}$ for doped RR100 are from F_4TCNQ crystals at the surface of the film.

This article is protected by copyright. All rights reserved.

2199160x, 2019, 11, Downloaded from https://onlinelibrary.wiley.com/doi/10.1002/aelm.201800915, Wiley Online Library on [22/02/2024]. See the Terms and Conditions (https://onlinelibrary.wiley.com/terms-and-conditions) on Wiley Online Library for rules of use; OA articles are governed by the applicable Creative Commons License

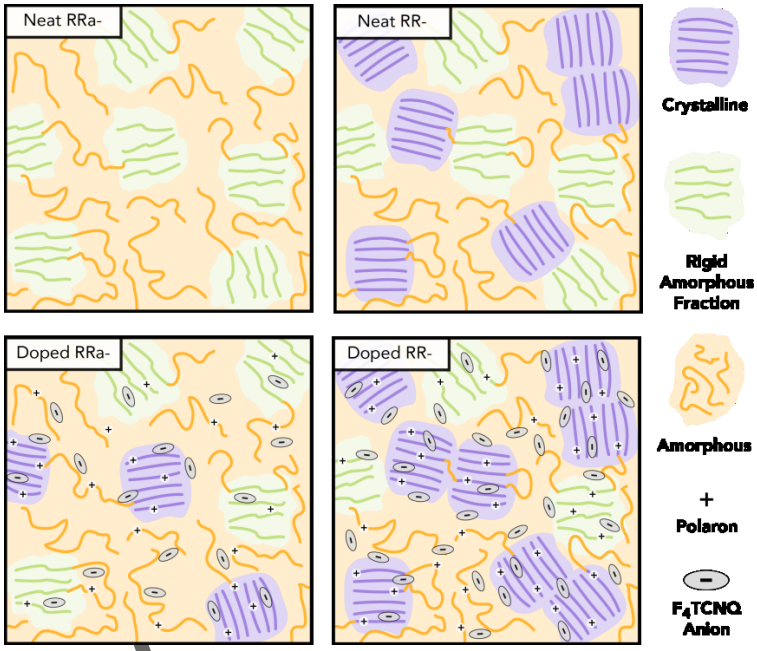

Figure 4. Schematic of neat and doped RR- and RRa-P3HT films showing morphological changes upon addition of F_4TCNQ at high concentration. Some of the regions in the RRa- films crystallize upon introduction of F_4TCNQ and we refer to these regions as rigid amorphous in the sense that they have some chain alignment without crystalline order.

Author Manuscript

This article is protected by copyright. All rights reserved.

2199160x, 2019, 11, Downloaded from https://onlinelibrary.wiley.com/doi/10.1002/aelm.201800915, Wiley Online Library on [22/02/2024]. See the Terms and Conditions (https://onlinelibrary.wiley.com/terms-and-conditions) on Wiley Online Library for rules of use; OA articles are governed by the applicable Creative Commons License

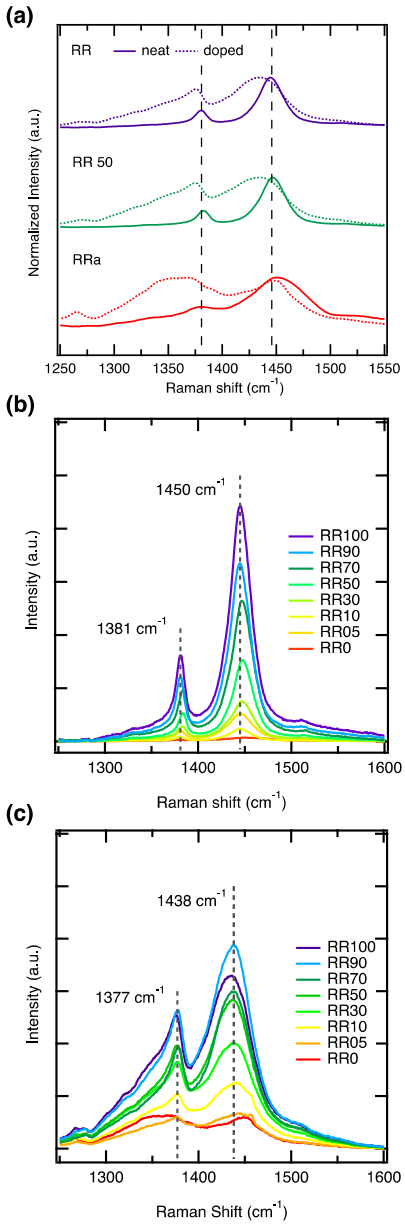

Figure 5. Raman spectra of **(a)** neat and doped RR, RR50, RRa films. Raman spectra of RR-:RRa-P3HT blends in **(b)** neat and **(c)** doped with F_4TCNQ forms excited at 633nm (off resonance with the neutral absorption of RR-P3HT).

Author

This article is protected by copyright. All rights reserved.

2199160x, 2019, 11, Downloaded from https://onlinelibrary.wiley.com/doi/10.1002/aelm.201800915, Wiley Online Library on [22/02/2024]. See the Terms and Conditions (https://onlinelibrary.wiley.com/terms-and-conditions) on Wiley Online Library for rules of use; OA articles are governed by the applicable Creative Commons License

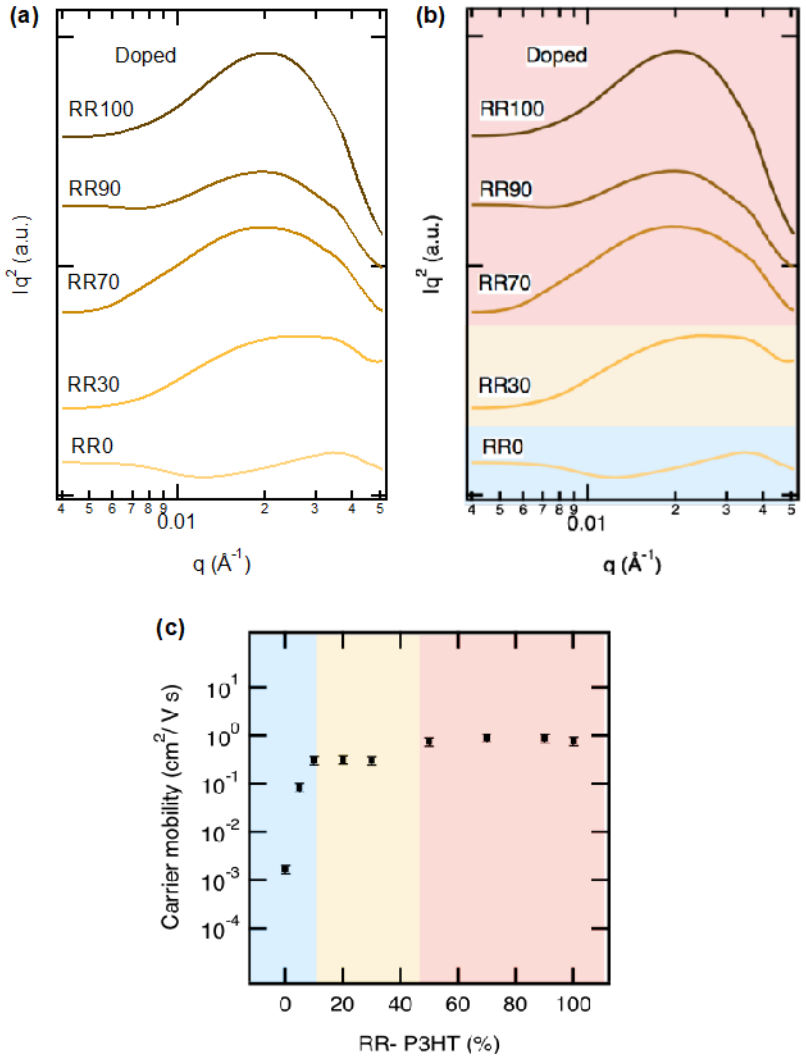

Figure 6. Lorentz corrected RSoXS profiles of **(a)** neat and **(b)** doped films of RR-:RRa-P3HT blends at resonant energy (285.4eV). **(c)** Carrier mobility as a function of % RR- P3HT. The highlighted regions in **(b)** and **(c)** correspond to same films.

Author

This article is protected by copyright. All rights reserved.

2199160x, 2019, 11, Downloaded from https://onlinelibrary.wiley.com/doi/10.1002/aelm.201800915, Wiley Online Library on [22/02/2024]. See the Terms and Conditions (https://onlinelibrary.wiley.com/terms-and-conditions) on Wiley Online Library for rules of use; OA articles are governed by the applicable Creative Commons License

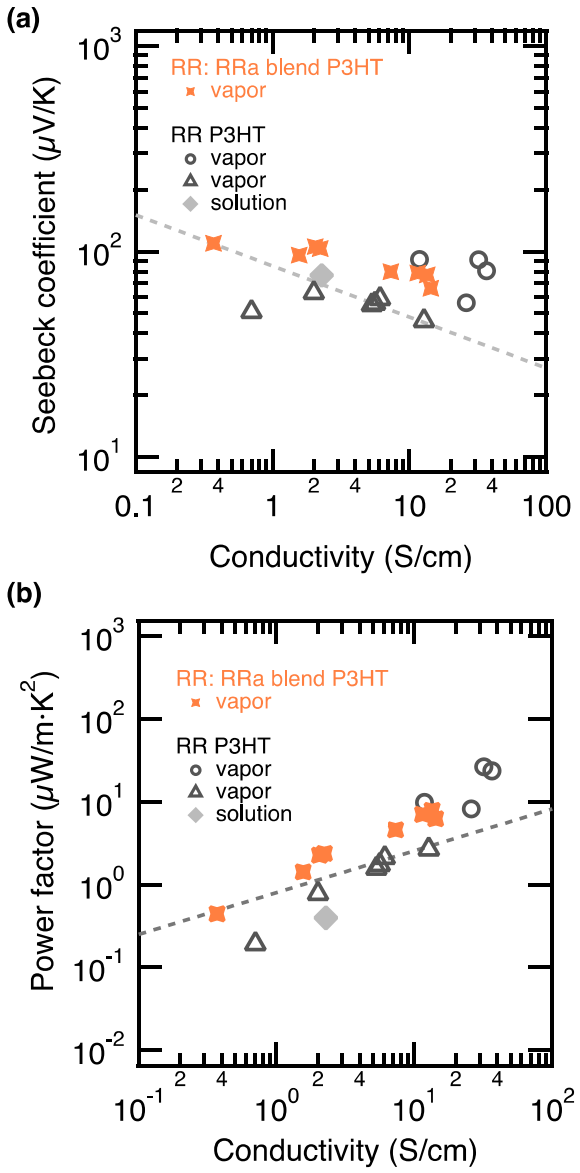

Figure 7. Thermoelectric properties of RR: RRa-P3HT blend films doped with F_4TCNQ from this study (orange) and 100% RR-P3HT films doped with F_4TCNQ using other doping methods. **(a)** Seebeck coefficient as a function of electrical conductivity shows that Seebeck is not a strong function of conductivity. **(b)** Power factor as a function of conductivity. Blend with higher %RR has higher electrical conductivity and power factor, and thus sits farther above the empirical trend line. Grey dotted lines represents empirical relationships, ($S \propto \sigma^{-\frac{1}{4}}$, $PF \propto \sigma^{\frac{1}{2}}$) [56] , grey circle: RR- P3HT film vapor doped with F_4TCNQ[65], grey triangle: RR- P3HT film casted from various solvents vapor doped with F_4TCNQ[17], and light grey filled diamond: RR- P3HT solution doped with F_4TCNQ[65]

Author Manuscript

This article is protected by copyright. All rights reserved.

2199160x, 2019, 11, Downloaded from https://onlinelibrary.wiley.com/doi/10.1002/aelm.201800915, Wiley Online Library on [22/02/2024]. See the Terms and Conditions (https://onlinelibrary.wiley.com/terms-and-conditions) on Wiley Online Library for rules of use; OA articles are governed by the applicable Creative Commons License

Author Manuscript

TOC TEXT

Blends of regioregular and regiorandom poly(3-hexylthiophene) doped with F_4TCNQ from the vapor phase have increasing thermoelectric performance with increasing fraction of regioregular polymer. Doping induces order in regiorandom P3HT due to stiffening of the backbone, but does not does not lead to an overall benefit in the performance of blends.

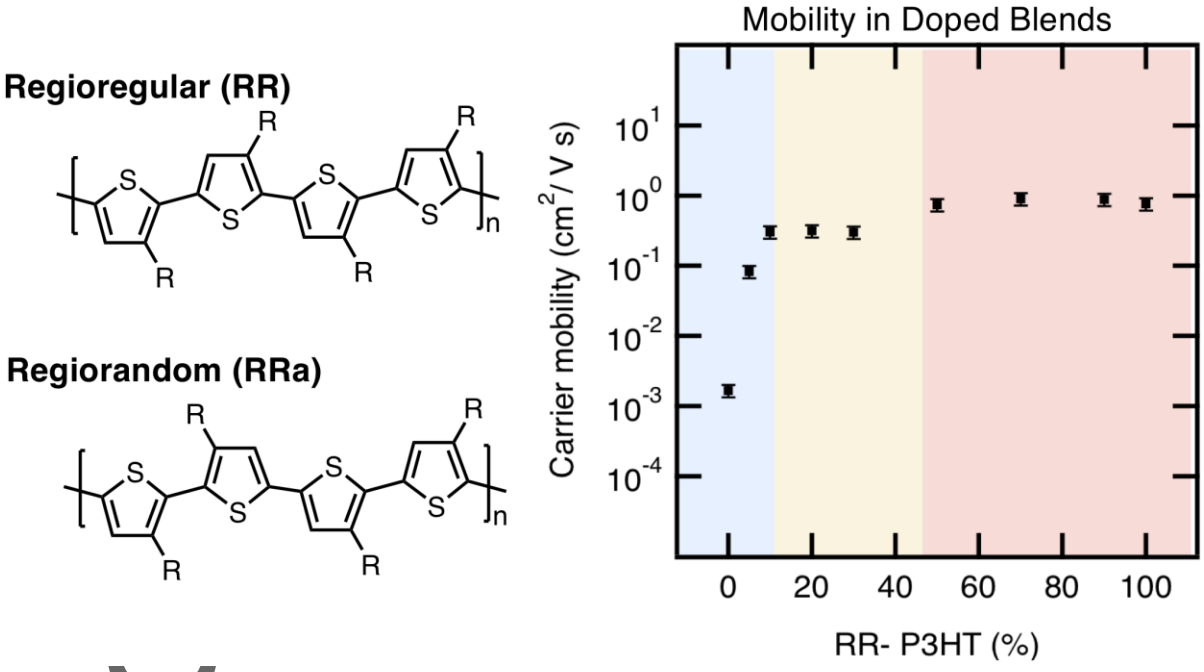

This article is protected by copyright. All rights reserved.

2199160x, 2019, 11, Downloaded from https://onlinelibrary.wiley.com/doi/10.1002/aelm.201800915, Wiley Online Library on [22/02/2024]. See the Terms and Conditions (https://onlinelibrary.wiley.com/terms-and-conditions) on Wiley Online Library for rules of use; OA articles are governed by the applicable Creative Commons License